

# Understanding carbonation in 3D printed cement-based materials with exposed bottom surface

Yi Zhang<sup>1,2</sup>, Kim Van Tittelboom<sup>1</sup>, Yaxin Tao<sup>1,3</sup>, Yiyuan Zhang<sup>1</sup>, Zhengwu Jiang<sup>2</sup>,  
Geert De Schutter<sup>1</sup>

<sup>1</sup> Magnel-Vandepitte Laboratory for Structural Engineering and Building Materials, Ghent University, Ghent, Belgium

<sup>2</sup> Key Laboratory of Advanced Civil Engineering Materials of Ministry of Education, School of Materials Science and Engineering, Tongji University, Shanghai, China

<sup>3</sup> Institute of Building Materials, ETH Zurich, Zurich, Switzerland

yi.zhang@ugent.be, kim.vantittelboom@ugent.be,  
yaxin.tao@ugent.be, yiyuan.zhang@ugent.be, jzhw@tongji.edu.cn,  
geert.deschutter@ugent.be

**Abstract.** Despite the continuously increasing scale and number of concrete 3D printing applications, current research on the durability of printed cement-based materials remains limited. The insufficient understanding of durability will hinder the widespread adoption and application of 3D printed cement-based materials in practical construction scenarios. In this study, the carbonation performance of printed samples, with exposure of the bottom surface, was assessed. A concave carbonation front is observed when the bottom side is exposed due to the non-uniform carbonation. This phenomenon is linked to the density gradient distribution of printed materials and is more pronounced with increased deformation of samples. Silica fume decreases the carbonation resistance of printed samples and leads to even more non-uniform carbonation.

**Keywords:** Durability, Carbonation, bottom surface, 3D printing.

## 1 Introduction

3D concrete printing technology has gained increasing attention in recent years due to its potential to address the challenges posed by the global population aging and global warming. This technology has transitioned from laboratory research to practical application, with increasing scale and number of applications [1,2]. In spite of this, it still faces numerous challenges [3,4]. The layer wise deposition process during printing introduces layer interface zones in 3D printed cement-based materials (3DPCM), significantly impacting their mechanical properties and durability [5,6]. The difference in mechanical properties of 3DPCM under various loading directions, i.e., anisotropy, was widely studied and reported [7,8]. On the contrary, research on the durability of 3DPCM is limited, which hampers the widespread adoption and application of 3DPCM in practical construction scenarios [9].

Carbonation of cement-based materials refers to the reaction between CO<sub>2</sub> and alkaline components (primarily calcium hydroxide) in the matrix under a proper moisture content [6,10]. As a result, the pH decreases, leading to faster corrosion of steel bars and shortening the service life of structures and buildings [10,11]. For 3D printed structures with flexural resistance requirements, steel bars are still one of the main means of reinforcement. Additionally, given the widespread occurrence of carbonation, it is essential to investigate and comprehensively understand the carbonation properties of 3DPCM. Zhang et al. [12] found the carbonation depth of printed samples is lower than that of cast samples. Malan et al. [13] and Van Der Putten et al. [6] also investigated the carbonation depth of printed samples. Nevertheless, they maintained the curved edge of the printed samples, resulting in a conflicting finding, i.e., a higher carbonation depth in printed samples with multilayer side (the vertical side parallel to the printing direction) exposed. They also discovered that the carbonation depth at the layer interface zone of samples printed without time interval was comparable to that at the bulk of layers. As the time interval increases, the carbonation depth at the layer interface zone significantly increases due to the accumulation of defects at the layer interface. Different from this, Sanchez et al. [14] also reported a preferential ingress of carbon dioxide at the layer interface zone in samples printed without time interval. In general, reported findings are limited and do not consider the carbonation anisotropy of printed samples.

In this study, the carbonation performance of printed samples with exposure of the bottom surface was investigated. Effects of silica fume and deformation on the carbonation performance were investigated. Furthermore, the pore distribution along the layer interface zone was characterized via X-ray computed tomography (CT) technology. It is expected to enhance the understanding of the carbonation performance of printed materials and facilitate the application of 3DPCM.

## 2 Experimental Program

### 2.1 Materials and Mix Proportions

CEM I 52.5 N Portland cement produced by Holcim according to the European Standard EN 197-1: 2011 [15] was adopted in this research. Silica fume (SF, 940-U, Elkem) was adopted as well. A liquid polycarboxylate superplasticizer (PCE) with a solid content of 35 % supplied by BASF (Master Glenium 51) was utilized. Quartz sand with a size range of 0 mm ~ 1 mm was used as aggregate. Hydroxypropyl methyl cellulose ether (HPMC) with a viscosity amounting to 30 Pa·s (Brookfield RV, 20 rpm, 1.9%, 20 °C) provided by Shin-Etsu (MOT 60,000 YP4) was used as thickener. Tap water was used as mixing water.

As shown in **Table 1**, the sand-to-cement ratio is 1. The water-to-cement ratio is 0.35. The mass ratio of HPMC to cement is 0.2%. The mass dosage of PCE was adjusted to maintain a similar slump flow for the two mixtures SF0 and SF10.

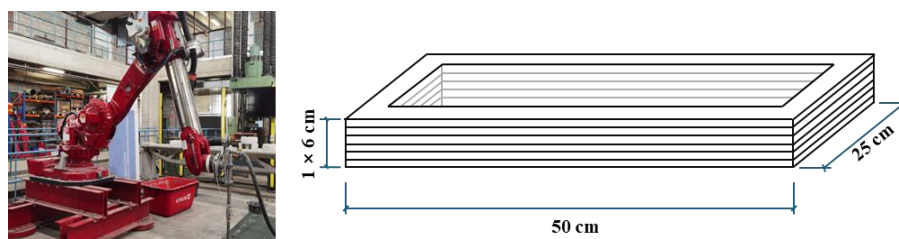
**Table 1.** Mix proportion of 3D printable cement-based materials (mass ratio)

No.	Cement	SF	Sand	Water	HPMC	PCE
SF0	1	0	1	0.35	0.2%	0.1%
SF10	0.9	0.1	1	0.35	0.2%	0.3%

## 2.2 Sample Preparation

The printable mixtures were prepared by a pan mixer. Firstly, raw materials including cement, SF (if any), sand and HPMC were dry mixed for 1 min at a rotation speed of 60 rpm. Afterwards, water and PCE were added and wet mixed for 3 min at the same rotation speed. Subsequently, the mixer was stopped for 1.5 min to scrape and homogenize materials manually. Finally, the mixture was mixed again for 2.5 min at 60 rpm.

The 3D printable mixtures were pumped and extruded using a screw pump. The length and diameter of the pipe amounted to 5 m and 25.4 mm. The diameter of the nozzle was 25.4 mm as well. The printing operation was conducted using a robotic arm moving at a velocity of 100 mm/s (**Fig. 1**). Rectangular contours with a width of 250 mm and a length of 500 mm were printed. The printed rectangular elements consisted of 6 layers with a thickness of 10 mm and a width of around 40 mm. Two printing procedures were adopted to obtain samples with different deformations. In the first type, six layers were printed continuously. In the second type, three layers were initially printed, followed by an additional three layers. The time interval, in between printing of each set of three layers, is the initial setting time (ASTM C807-13) of the materials. The samples printed with and without time interval were denoted as  $T_0$  and  $T_{set}$ , respectively. After printing all 6 layers, printed elements were covered with plastic foil for 1 day. Subsequently, the printed elements were moved to a curing room with a temperature of  $20\text{ }^{\circ}\text{C} \pm 2\text{ }^{\circ}\text{C}$  and a relative humidity of  $60\% \pm 5\%$ .

**Fig. 1.** Illustration of 3D printer and printed elements.

## 2.3 Carbonation Test

Samples with a width of 5 cm were extracted from the printed elements at the age of 28 d, and then these samples were dried at  $40\text{ }^{\circ}\text{C}$  until the mass loss over 24 h was less than 0.1%. Thereafter, 5 sides of these samples were coated with epoxy resin (Episol Designtop SF, Resiplast NV), leaving the bottom side as the exposure surface. When

the epoxy resin was dried, the samples were moved to the carbonation chamber maintained at 20 °C with a relative humidity of 60% and a 2% CO<sub>2</sub> concentration. The exposure time was 7 d and 90 d. Three samples were measured for each series at each exposure age.

The carbonated samples were split into 2 parts when they reached the measuring age. Subsequently, phenolphthalein solution with a concentration of 1% was sprayed on the freshly split surface of each part. Around 30 minutes after spraying the phenolphthalein solution, photographs of each split surface along with a scale were taken. The carbonation depth was measured by Image J [6]. To minimize the effects introduced by the variation in the section area of samples during carbonation, only the carbonation depth in the area within the width of 40 mm in the center of samples was measured (**Fig. 2**).

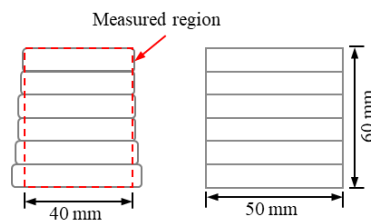


**Fig. 2.** Illustration of sample size and measured region.

## 2.4 Microstructure Analysis

X-ray computed tomography (CT) was used to characterize the pore distribution in samples. Cylindrical specimens with a diameter of 28 mm and a height of 40 mm were drilled from the printed rectangular samples. The drill direction was horizontal and perpendicular to the printing direction. Scanning was performed using a TESCAN CoreTOM CT system, and this resulted in a voxel size of 56  $\mu\text{m}$ . Samples were scanned by the X-rays at a voltage of 180 keV and a 0.5 mm Cu filter was used. 3D structural information of the samples was obtained by reconstructing all tomographic images acquired for each sample using Panthera software. This procedure employed a ring filter with a width of 10 Hounsfield units and an arc degree of 360°. The reconstructed 3D information of the samples was visualized and analyzed using Avizo software.

## 3 Results and Discussions

### 3.1 Carbonation Penetration

**Fig. 3** presents the carbonation front in samples at 7 d. It can be found that the carbonation front in all samples is concave. Additionally, a higher carbonation depth is measured at the edge of samples than that measured at the center of samples (**Fig. 4**). This phenomenon is unlikely that the lack of sealing, but indicates a non-uniform

carbonation along the bottom surface, demonstrating by the significant difference between different mixtures. This phenomenon can be ascribed to the gradient distribution of density in printed samples [16]. On the one hand, the lack of consolidation during deposition without formwork contributes to a lower density near the edge of printed samples. Additionally, the large deformation at bottom layers results in an increased exposure surface. On the other hand, samples were printed continuously (at least 3 layers) without time intervals. Therefore, defects partly caused by drying shrinkage at the layer interface are mainly restricted to the edges of printed samples. Consequently, the penetration rate of CO<sub>2</sub> and moisture near the sample edge is higher than that at the center of samples.

It is interesting to observe that samples printed without time intervals have a more obvious concave carbonation front despite the weaker evaporation and smaller shrinkage due to the foil covering (**Fig. 3**). The carbonation depth variation along the sample width also increases when the samples were printed at a setting time interval (**Fig. 4** and **Table 2**). It can be explained by the fact that the higher deformation at the bottom layers of printed samples without time intervals intensifies the density gradient distribution. In the contrary, the lower deformation in bottom layers of samples printed with time interval improves the uniformity of printed samples along the width. It should be mentioned that the carbonation depth does not exceed 30 mm (height of 3 layers) even after 90 d exposure. Therefore, the cold joint at the layer interface due to the initial time interval can be ignored.

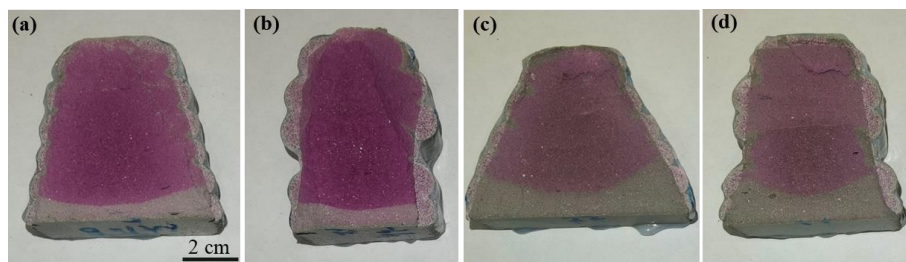


**Fig. 3.** Carbonation front of samples at 7 d: (a) SF0-T<sub>0</sub>, (b) SF0-T<sub>set</sub>, (c) SF10-T<sub>0</sub>, (d) SF10-T<sub>set</sub>.

**Table 2.** Carbonation depth of samples

No.	Mean (mm)		Maximum (mm)		Minimum (mm)	
	7 d	90 d	7 d	90 d	7 d	90 d
SF0-T <sub>0</sub>	7.7	10.0	9.2	11.0	6.8	9.2
SF0-T <sub>set</sub>	7.3	9.1	7.9	9.6	6.6	8.6
SF10-T <sub>0</sub>	12.1	17.7	15.7	23.4	10.3	14.3
SF10-T <sub>set</sub>	12.2	14.2	15.5	17.7	9.9	12.4

We note that the addition of SF increases the carbonation depth and increases the discrepancy between the maximum carbonation depth and the minimum carbonation depth (**Table 2**). The mean carbonation depth of SF10-T<sub>0</sub> exposed to CO<sub>2</sub> for 7 d and

90 d amount to 12.1 mm and 17.7 mm, which is 57% and 77% higher than that of SF0-T<sub>0</sub>, respectively. This indicates SF decreases the carbonation resistance of samples and enhances the non-uniform carbonation phenomenon. The enhanced density gradient distribution as well as the increased exposure area due to the higher deformation at bottom layers contribute to this phenomenon. Nevertheless, the more important reason is the decrease in pH of the pore solution caused by secondary hydration of SF [17,18]. This can be demonstrated by the much higher carbonation depth and more obvious concave carbonation front in SF10-T<sub>set</sub> than that in SF0-T<sub>0</sub>. As the exposure time increases, the carbonation depth increases. In addition, the uniformity of the carbonation in printed samples increases except for series SF10-T<sub>0</sub>, which is evidenced by the lower variation in carbonation depth along the sample width. This can be attributed to the large deformation of SF10-T<sub>0</sub>, resulting in a higher variation in the sample width with sample height.

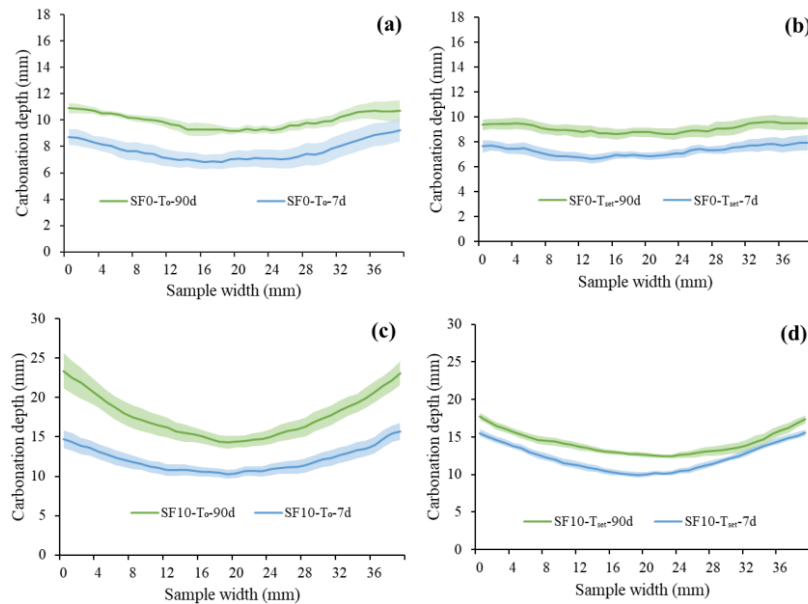


**Fig. 4.** Carbonation depth of samples at different exposure times: (a) SF0-T<sub>0</sub>, (b) SF0-T<sub>set</sub>, (c) SF10-T<sub>0</sub>, (d) SF10-T<sub>set</sub>. (error bars represent standard error, n=6) .

### 3.2 Pore Distribution

From **Fig. 5**, it is evident that the porosity is higher and more large pores are present near the edge of printed samples, especially at the layer interface zone. As it comes to the center, the porosity decreases, i.e., showing a density gradient distribution. This observation can be attributed to material deformation after extrusion. The materials deform under the extrusion pressure and self-weight without the restriction of formwork, resulting in a higher density at the center compared to that at the edge. This also causes a larger height of extruded layers at the center than that near the edge. With

the continuous printing of subsequent layers, the contact and interaction between layers at the center is stronger than that at the edge. Hence, it further enlarges the difference in the density between the edge and center of the layer interface zone in printed samples. Moreover, aggregates migrate into the material during printing due to the wall effect, leading to the formation of a lubrication layer. This contributes to this phenomenon as well [19].

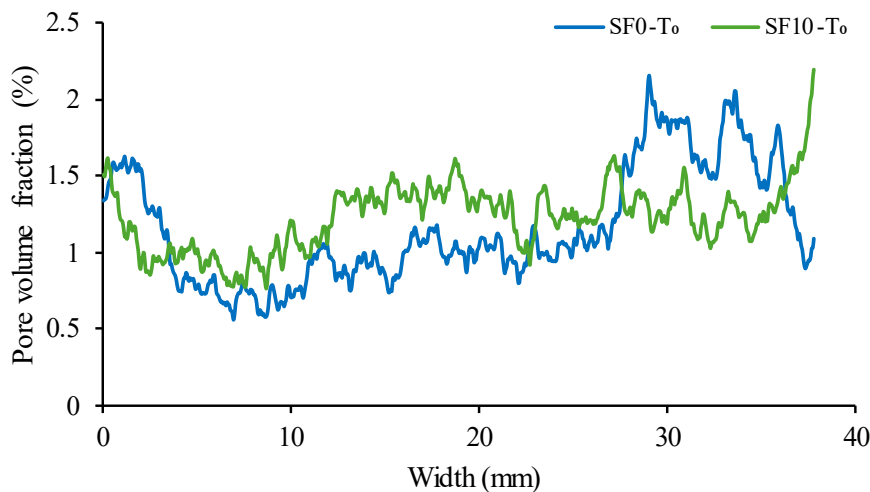


**Fig. 5.** Porosity distribution along sample width observed by CT

## 4 Conclusions

Based on the above results, the conclusions can be drawn as follows:

- (1) The non-uniform carbonation due to the density gradient distribution in printed samples results in a concave carbonation front in printed samples with the bottom side exposed.
- (2) The carbonation uniformity and resistance of samples printed without time interval decrease owing to the enhanced density gradient distribution caused by the higher deformation at bottom layers.
- (3) Silica fume increases the carbonation depth of printed samples and decreases the carbonation uniformity, caused by the higher deformation and decreased pH due to secondary hydration reactions.

## References

1. Ma G, Buswell R, Da Leal Silva WR, Wang L, Xu J, Jones SZ: Technology readiness: A global snapshot of 3D concrete printing and the frontiers for development. *Cem. Concr. Res.* 156, 106774 (2022).

2. Zhang Y, Ren Q, Dai X, Tao Y, Zhang Y, Jiang Z et al.: A potential active rheology control approach for 3D printable cement-based materials: Coupling of temperature and viscosity modifiers. *Cem. Concr. Compos.*, 105496 (2024).
3. De Schutter G, Lesage K, Mechtcherine V, Nerella VN, Habert G, Agusti-Juan I: Vision of 3D printing with concrete — Technical, economic and environmental potentials. *Cem. Concr. Res.* 112, 25–36 (2018).
4. Zhang Y, Jiang Z, Zhu Y, Zhang J, Ren Q, Huang T: Effects of redispersible polymer powders on the structural build-up of 3D printing cement paste with and without hydroxypropyl methylcellulose. *Constr. Build. Mater.* 267, 120551 (2021).
5. Wolfs R, Bos FP, Salet T: Hardened properties of 3D printed concrete: The influence of process parameters on interlayer adhesion. *Cem. Concr. Res.* 119, 132–40 (2019).
6. van der Putten J, Volder M de, van den Heede P, Deprez M, Cnudde V, Schutter G de et al.: Transport properties of 3D printed cementitious materials with prolonged time gap between successive layers. *Cem. Concr. Res.* 155, 106777 (2022).
7. Nerella VN, Hempel S, Mechtcherine V: Effects of layer-interface properties on mechanical performance of concrete elements produced by extrusion-based 3D-printing. *Constr. Build. Mater.* 205, 586–601 (2019).
8. Tao Y, Mohan MK, Rahul AV, Yuan Y, De Schutter G, Van Tittelboom K: Stiffening controllable concrete modified with redispersible polymer powder for twin-pipe printing. *Cem. Concr. Res.* 161, 106953 (2022).
9. Nodehi M, Aguayo F, Nodehi SE, Gholampour A, Ozbakkaloglu T, Gencel O: Durability properties of 3D printed concrete (3DPC). *Autom. Constr.* 142, 104479 (2022).
10. Ashraf W: Carbonation of cement-based materials: Challenges and opportunities. *Constr. Build. Mater.* 120, 558–70 (2016).
11. Šavija B, Luković M: Carbonation of cement paste: Understanding, challenges, and opportunities. *Constr. Build. Mater.* 117, 285–301 (2016).
12. Zhang Y, Zhang Y, Yang L, Liu G, Chen Y, Yu S et al.: Hardened properties and durability of large-scale 3D printed cement-based materials. *Mat. Struct.* 54(1), 1–14 (2021).
13. Malan JD, van Rooyen AS, van Zijl, Gideon P. A. G.: Chloride Induced Corrosion and Carbonation in 3D Printed Concrete. *Infrastructures* 7(1), 1 (2022).
14. Sanchez AMA, Wangler T, Stefanoni M, Angst U: Microstructural examination of carbonated 3D-printed concrete. *J Microsc* 286(2), 141–7 (2022).
15. BS EN 197-1. Cement—Part 1: Composition, specifications and conformity criteria for common cements. British Standards Institution; 2011.
16. Zhang Y, Zhu Y, Ren Q, He B, Jiang Z, Van Tittelboom K et al.: Comparison of printability and mechanical properties of rigid and flexible fiber-reinforced 3D printed cement-based materials. *Constr. Build. Mater.* 400, 132750 (2023).
17. Kulakowski MP, Pereira FM, Molin DCD: Carbonation-induced reinforcement corrosion in silica fume concrete. *Constr. Build. Mater.* 23(3), 1189–95 (2009).
18. Turk K, Karatas M, Gonen T: Effect of Fly Ash and Silica Fume on compressive strength, sorptivity and carbonation of SCC. *KSCE J Civ Eng* 17(1), 202–9 (2013).
19. van der Putten J, Deprez M, Cnudde V, De Schutter G, Van Tittelboom K: Microstructural Characterization of 3D Printed Cementitious Materials. *Materials* 12(18) (2019).